Long-Range Guanine Oxidation in DNA Restriction Fragments by a Triplex-Directed Naphthalene Diimide Intercalator†

Megan E. Núñez,‡ Katherine T. Noyes,‡ Diego A. Gianolio,§ Larry W. McLaughlin,*,§ and Jacqueline K. Barton*,‡

Division of Chemistry and Chemical Engineering, California Institute of Technology, Pasadena, California 91125, and Department of Chemistry, Merkert Chemistry Center, Boston College, Chestnut Hill, Massachusetts 02467

Received February 7, 2000; Revised Manuscript Received March 20, 2000

ABSTRACT: Naphthalene diimide (NDI), a powerful oxidant that binds avidly to DNA by intercalation, is seen to damage the 5′ guanine of 5′-GG-3′ sites by photoactivated charge transport through DNA. When covalently tethered to the center of a triplex-forming oligonucleotide and delivered by triplex formation within a pyrimidine•purine-pyrimidine motif to a specific site on a restriction fragment, NDI can photooxidize guanine over at least 25−38 bp in each direction from the site of binding. Charge migration occurs in both directions from the NDI intercalator and on both DNA strands of the target, but the oxidation is significantly more efficient to the 3′ side of the triplex. NDI and octahedral rhodium intercalators, when tethered directly to the 5′ terminus of the triplex-forming strand as opposed to the center, generate significant amounts of oxidative damage only in the immediate vicinity of the intercalation site. Given that long-range charge transport depends on DNA stacking, these results suggest that the base stack is distorted at the 5′ end of the triplex region in the duplex−triplex junction. Targeting of photooxidative damage by triplex formation extends our previous studies of long-range charge transport to significantly longer DNA sequences through a strategy that does not require covalent attachment of the photooxidant to the DNA being probed. Moreover, triplex targeting of oxidative damage provides for the first time a typical distance distribution for genomic charge transport of ∼200 Å around the oxidant.

The stacked bases of the DNA double helix provide an efficient medium for charge transport, as revealed by a variety of spectroscopic, electrochemical, and biochemical methods (*1*). DNA can act both as a conduit for the migration of charge within a donor−acceptor pair and as a reactant in the charge transfer chemistry. Photoexcited rhodium(III) intercalators bound covalently to one terminus of an oligodeoxynucleotide were shown first to oxidize the 5′ guanine of 5′-GG-3′ sites from a distance (*2*). Guanines are oxidized preferentially because they have the lowest oxidation potential of the nucleotide bases (*3*), and the selectivity for 5′ guanines of guanine doublets is proposed to arise from the effects of base stacking on the ionization potentials of the bases (*4*, *5*) so that the oxidation potentials increase across the series as follows: 5′-GG-3′ > 5′-GA-3′ ≫ 5′-GC-3′ and 5′-GT-3′. This 5′ guanine reactivity has become the characteristic signature of DNA electron transfer, and can be used to distinguish between charge transfer chemistry and singlet oxygen chemistry, which damages all guanines indiscriminately (*2*, *6*). The efficiency of this long-range guanine oxidation is directly influenced by the coupling of the oxidant into the π-stack and by the degree of stacking of the intervening base pairs (*2*, *7*). Moreover, the efficiency of DNA-mediated oxidation displays a very shallow dependence on distance (*8*). Most importantly, it has become clear that this long distance charge transfer chemistry is a general feature of double-helical DNA and not of the oxidant; Ru(III) intercalators (*9*), as well as organic molecules such as ethidium (*10*) and anthraquinones (*11*, *12*), have also been shown to oxidize guanine doublets from a distance.

It is currently thought that long-range oxidative damage to DNA involves first injection of the electron hole into the base pair stack, migration of the hole through the duplex, and, finally, irreversible damage to the guanine base. Site-specific injection is commonly initiated by photoactivation of a tethered, stacked oxidant. Proposals for how migration through the base pair stack occurs include hopping (*13*), polaron formation (*11*), and tunneling; some combination of these mechanisms is likely involved (*14*). It is clear, however, that equilibration of the radical occurs on the basis of oxidation potential across the duplex. The guanine radical has been detected within the duplex by transient absorption spectroscopy and has a lifetime of ∼100 μs (*15*). On this time scale, irreversible trapping of the radical with H_2O and O_2 occurs, which yields a mixture of oxidation products (*6*, *16*−*19*).

We previously demonstrated that charge migration on oligonucleotide duplexes can yield permanent base lesions at distances of at least tens of base pairs from the damaging agent. We are interested in considering whether and how these holes might also migrate along DNA within the cell to distribute damage across the genome. This possibility

† This work was supported by grants from the NIH (GM53210 to L.W.M. and GM49216 to J.K.B.), as well as funding from the National Foundation for Cancer Research, the Howard Hughes Medical Institute predoctoral fellowship program (M.E.N.), and the Caltech SURF program (K.T.N.).

* To whom correspondence should be addressed. E-mail: larry.mclaughlin@bc.edu or jkbarton@caltech.edu.

‡ California Institute of Technology.

§ Boston College.

10.1021/bi000285s CCC: $19.00
Published on Web 04/26/2000

holds implications both for the generation of damage on DNA and for its repair (*20*). In this context, it is important to determine the distance range for charge transport in natural DNA sequences. Here we begin to explore this question by examining the distribution of damage along a DNA restriction fragment through the site-specific targeting of a naphthalene diimide intercalator using oligonucleotide-directed triplex formation.

It has long been known that naphthalene diimide (NDI)[1] molecules intercalate into DNA (*21*−*24*), and are potent electron acceptors (*25*−*28*). Matsugo et al. showed that hydroperoxy derivatives of naphthalene diimide molecules oxidize guanine with a preference for 5′ guanines (*29*). They attributed this damage to the generation of hydroxyl radicals from the hydroperoxy groups on the basis of control experiments that showed that these functional groups were necessary for DNA cleavage to occur. It was later demonstrated that the related noncovalent naphthalimide molecule lacking the hydroperoxy groups exhibited the same preference for 5′ guanines, and this preference was attributed to electron transfer chemistry (*30*). Recently, the triplet excited states of photoexcited naphthalene diimide molecules were shown to oxidize nucleotides in aqueous solution, with oxidation of GMP being by far the most efficient (*31*, *32*). The reduction potential of the triplet excited state was estimated to be 1.8 V versus NHE, high enough to oxidize all of the nucleotide bases. In this study, we demonstrate that naphthalene diimide (NDI) intercalators covalently tethered to DNA sequences can oxidize guanine *at long range*, and we exploit the chemistry of this intercalator to examine the limits of charge transfer in DNA restriction fragments.

Since NDI and other intercalating photooxidants bind to DNA in a relatively sequence-neutral fashion (*21*), we tethered NDI to a second molecule which confers upon it sequence specificity, in this case a triplex-forming oligonucleotide (TFO). Triple helices are formed by the binding of a single-stranded oligonucleotide in the major groove of duplex DNA (*33*). These third strand oligonucleotides bind most tightly to sequences that contain only purines on one strand of the Watson−Crick duplex and only pyrimidines on the other. In the pyrimidine motif used in this study, an oligopyrimidine third strand binds parallel to the purine strand of the duplex, forming Hoogsteen hydrogen bonds between the duplex guanine and the protonated cytosine of the third strand (C^+·GC), and between the duplex adenine and the thymine of the third strand (T·AT). Triple helices have been shown to bind specifically to their target sequences on both short nucleotides and plasmid vectors, with association constants on the order of 10^7 M^{-1} depending on sequence, salt concentration, temperature, and pH (*34*−*37*). Furthermore, molecules that react with DNA have been attached to a triple-helix-forming oligonucleotide and delivered site-specifically to their target (*38*, *39*). NDI intercalators covalently tethered to triplex-forming oligonucleotides stabilize the triplex considerably (*40*−*42*). By attaching our naphthalene diimide intercalator to a 16 bp triplex-forming oligonucleotide, we have selectively targeted it to a single site on a restriction fragment and have determined the extent and pattern of base damage generated by this new photooxidant on a long piece of genomic DNA.

[1] Abbreviations: NDI, naphthalene diimide; TFO, triplex-forming oligonucleotide; phi, phenanthrenequinone diimine; DMB, 4,4′-dimethyl-2,2′-bipyridine; bpy′, 4-butyric acid 4′-methylbipyridine; NHE, normal hydrogen electrode.

MATERIALS AND METHODS

Oligonucleotide Preparation. Preparation of oligonucleotides with appended naphthalene diimides has been described (*40*−*42*). The synthesis and purification of $Rh(phi)_2bpy'^{3+}$ and of unmodified oligonucleotides have also been described in detail elsewhere (*43*).

Preparation of Restriction Fragments with Triplex-Binding Sites. Triplex-binding oligonucleotides with *Eco*RI or *Bam*HI sticky ends and 5′ phosphate termini were synthesized by standard phosphoramidite chemistry on an Applied Biosystems DNA synthesizer. These strands were purified twice by HPLC, annealed, and ligated into the dephosphorylated *Bam*HI site or *Eco*RI site of pUC19 by incubation with T4 DNA ligase at 16 °C overnight (New England Biolabs). This plasmid was transfected into commercially available DH5α competent *Escherichia coli* (Life Technologies) by standard methods (*44*), and the cells were plated out on LB plates containing ampicillin, X-Gal, and IPTG (Aldrich, Boerhinger-Mannheim). Cultures were innoculated from separate clear colonies, and the plasmids were isolated (Qiagen) and sequenced by the Caltech DNA sequencing facility.

End Labeling of Restriction Fragments. End-labeled restriction fragments were prepared by standard methods. Briefly, 20 μg of plasmid was cut with the first restriction enzyme, dephosphorylated using shrimp alkaline phosphatase (Boerhinger-Mannheim), phenol/chloroform extracted, and ethanol precipitated. Then the DNA was end-labeled using [γ-^{32}P]ATP (ICN) and polynucleotide kinase (New England Biolabs) or [α-^{32}P]ATP (Amersham) and terminal transferase (Boerhinger-Mannheim). This DNA was again phenol/chloroform extracted and ethanol precipitated before being digested with the second restriction enzyme. The desired fragment was isolated by nondenaturing polyacrylamide gel electrophoresis, identified by autoradiography, extracted by crushing and soaking in 10 mM Tris-HCl with 1 mM EDTA, and purified on a C18 minicolumn (Nensorb).

Triplex Annealing. The following mixtures were supplemented with the desired concentration of triplex-forming oligonucleotide: Rh triplexes, 50 mM MES buffer (pH 5.75), 10 mM $MgCl_2$, 1 mM spermidine chloride (Aldrich), 75 μM (base pair) calf thymus DNA (Boerhinger-Mannheim), and the minimum amount of radiolabeled DNA required for visualization of the samples; and NDI triplexes, "Wide Range" phosphate/citrate buffer (9.5 mM citrate and 12.5 mM phosphate) (pH 5.6), 10 mM $MgCl_2$, 1 mM spermidine chloride (Aldrich), 75 μM (base pair) calf thymus DNA (Boerhinger-Mannheim), 1−2 molar equiv of triplex-binding oligonucleotide, and the minimum amount of radiolabeled DNA required for visualization of the samples. The samples were allowed to equilibrate for at least 12 h at 4 °C and were irradiated at a controlled temperature.

Irradiation and Visualization of Samples. Samples (∼30 μL) were irradiated in the annealing buffer at 11 ± 1 °C at the desired wavelength on a 1000 W Hanovia Hg−Xe arc lamp equipped with a monochromator. After irradiation, the

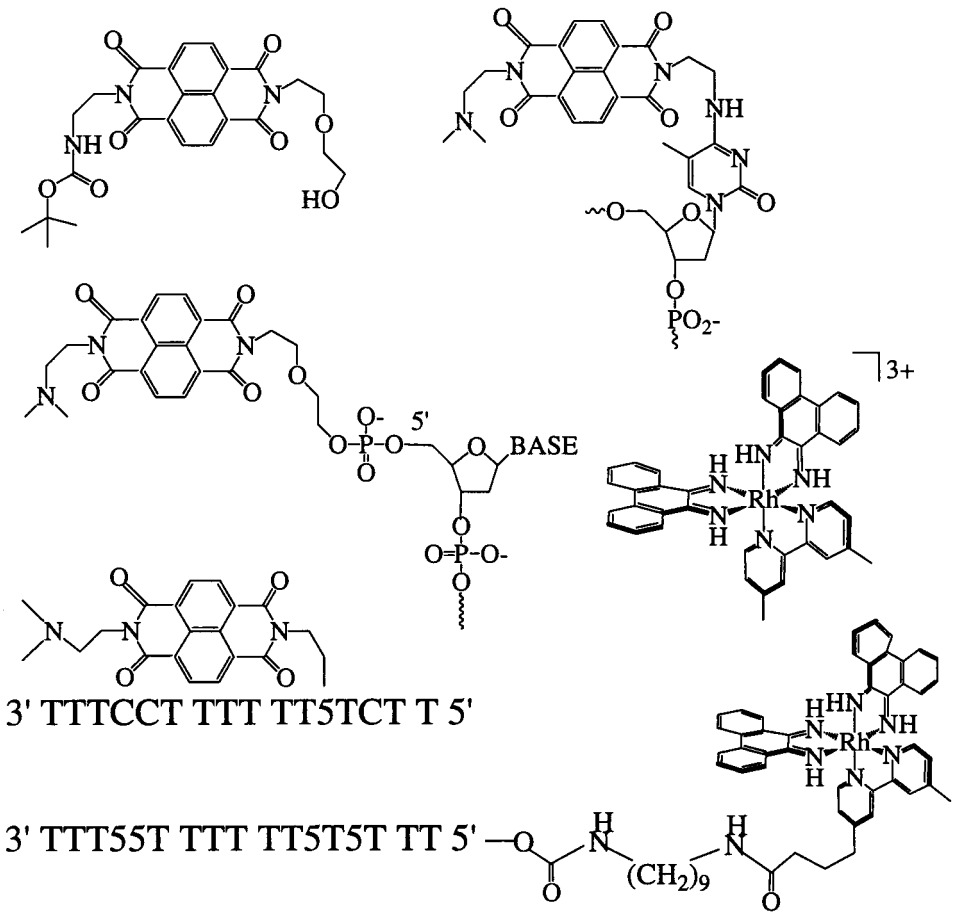

FIGURE 1: Structures of the intercalating photooxidants and oligonucleotide conjugates used in this study. At top left is the naphthalene diimide molecule in the noncovalent form. On the right is the cytosine-tethered naphthalene diimide molecule, which can be prepared as a phosphoramidite and incorporated into an oligonucleotide according to standard solid-phase methods (*33*). In the middle is the 5′-tethered NDI, attached to the sugar−phosphate backbone through a five-atom linker (*34*), and the $Rh(phi)_2DMB^{3+}$ octahedral metallointercalator, a strong photooxidant which has been shown to damage guanine bases at long range through the DNA base stack (*2*). On the bottom are shown two of the intercalator−oligonucleotide conjugates. "5" represents 5-methylcytosine.

DNA was ethanol precipitated to remove as much spermidine chloride and magnesium chloride as possible. The DNA was then cleaved by incubation in 100 μL of 10% piperidine for 30 min at 90 °C and dried in vacuo. Samples were analyzed by denaturing polyacrylamide electrophoresis on a 6% gel, followed by visualization and quantitation by phosphorimagery (ImageQuant by Molecular Dynamics).

RESULTS

Intercalator−DNA Conjugates. A 17-mer pyrimidine triplex-forming oligonucleotide was prepared with $Rh(phi)_2bpy'^{3+}$ appended to the 5′ end of the sugar−phosphate backbone by a nine-carbon linker. Two naphthalene diimide (NDI) conjugates with a pyrimidine 16-mer oligonucleotide were also prepared for these studies. In the first, the intercalator was attached to the 5′ end of the sugar−phosphate backbone through a short linker and a phosphodiester, and in the second, the intercalator was attached directly to the N4 amino group of a methylated cytosine base incorporated into the base sequence. These conjugates, along with $Rh(phi)_2DMB^{3+}$ and protected, noncovalent NDI, are illustrated in Figure 1.

Targeting $Rh(phi)_2bpy'^{3+}$ to a Single Specific Sequence by Triplex Formation. Although $Rh(phi)_2bpy'^{3+}$ intercalates avidly into DNA, its binding is largely sequence-neutral (*45*). To confer sequence specificity to the intercalator, we tethered it to a pyrimidine triplex-forming oligonucleotide (TFO), and we incorporated a specific binding site at two locations within the plasmid pUC19 for the TFO to target (Figure 2).

When the metallointercalator−TFO conjugate was incubated with a restriction fragment containing the target sequence, the rhodium complex was delivered to the target site and bound to the duplex adjacent to the triplex region. We established the binding site of the 5′-tethered rhodium complex by direct photocleavage of the sugar−phosphate backbone using 313 nm irradiation (*2*, *45*). Specific binding to the target site and concomitant photocleavage were observed from 8 μM down to less than 16 nM rhodium triplex strand (Figure 3). Furthermore, no nonspecific damage was observed, even at 8 μM triplex-forming oligonucleotide. The fact that the triplex-forming oligonucleotide was bound to the target site and not elsewhere on the restriction fragment at a concentration of ~1 μM was confirmed by DNase I footprinting experiments, in which a clear footprint was observed in the triplex region in both the absence and presence of tethered metallointercalator (data not shown).

Having established that the 5′-Rh-tethered TFO binds specifically to its target site, we irradiated the conjugate with its target restriction fragment and observed piperidine-sensitive damage in the same region as the direct photo-

Sequence 1

```
5'GCAGGATCCCCGGGTACCGAGCTCGAATTCTTTCCTTTTTTCTCTTTGAATTCACTGGCCGTCGTTTTACAACGTCGTG3'  Pyr
3'CGTCCTAGGGGCCCATGGCTCGAGCTTAAGAAAGGAAAAAAGAGAAACTTAAGTGACCGGCAGCAAAATGTTGCAGCAC5'  Pur
                              3' TTT55TTTTTT5T5TTT 5'                                  TFO
                3' side                                          5' side
                                                  Rh
```

Sequence 2

```
5'TGCCTGCAGGTCGACTCTAGAGGGATCCAGTTTCCTTTTTTCTCTTTACGACTGTAGCCGAGATCAGCCGCTAACGCCG3'  Pyr
3'ACGGACGTCCAGCTGAGATCTCCCTAGGTCAAAGGAAAAAAGAGAAATGCTGACATCGGCTCTAGTCGGCGATTGCGGC5'  Pur
                              3' TTTCCTTTTTT5TCTT 5'                                   TFO
              3' side                                  5' side
                                        NDI
```

FIGURE 2: Sequence of the designed restriction fragments used in this study, showing only the part of the fragment flanking the target polypurine-polypyrimidine site. The restriction fragments used in this study are in fact considerably longer than these sequences by approximately 200 bp. A 5′-tethered and a base-tethered intercalator−TFO conjugate are also shown. Note that both TFOs can bind to both restriction fragments, since both sequences contain the identical target site and differ only in their flanking sequence. "5" represents 5-methylcytosine. The terms "5′ side" and "3′ side" refer to the direction along the duplex relative to the orientation of the third strand, and "PUR" and "PYR" refer to the purine-rich and pyrimidine-rich target duplex strands, respectively.

cleavage. However, we observed little or no long-range damage (Figure 4), in contrast to that seen repeatedly on oligonucleotide duplexes (*2*, *7*, *8*). Proposing that the metal complex was not well-intercalated into the duplex DNA, we systematically changed the length of the tether, the orientation of the linker ligand, the composition of the buffer, the chirality of the metal center, and the sequence of the putative intercalation site. In addition, we examined base oxidation by a 5′-tethered Ru(phen)(bpy′)(dppz)$^{3+}$ complex. In all cases, we observed a pattern of damage localized to the duplex−triplex junction at the 5′ end of the triplex (data not shown).

Oxidation of 5′-GG-3′ Sites in DNA Duplexes by Naphthalene Diimide Intercalators. We examined first photooxidation on a 22 bp oligonucleotide duplex by noncovalent naphthalene diimide (Figure 5a). The target sequence contained two 5′-GG-3′ sites. Selective oxidation at the 5′ guanines of both guanine doublets was observed when the mixture was irradiated at 313, 340, and 365 nm but not at 400 nm (Figure 5b). Absorption maxima for NDI are at 340, 358, and 378 nm. For subsequent work, irradiations were conducted at 365 nm, since this wavelength provides a high intensity from the lamp, yields a low level of background DNA damage, and has been used for other photooxidation experiments. Base damage was revealed upon cleavage of the DNA at the lesion with hot aqueous piperidine. Some oxidation was also observed at a single guanine positioned near the end of the sequence.

We compared this oxidative damage to that generated by photoexcited Rh(phi)$_2$bpy′$^{3+}$ covalently tethered to the 5′ end of the same duplex, and we found that the oxidation pattern was strikingly similar to that generated by noncovalent NDI. When both oxidants were present simultaneously, the amount of damage generated at guanines was diminished but not eliminated, which may be due to oxidation of NDI by photoexcited Rh(phi)$_2$bpy′$^{3+}$. To demonstrate that the similarity in the pattern of oxidation was not fortuitous, we compared also the pattern of base oxidation generated by noncovalent NDI and noncovalent Rh(phi)$_2$DMB^{3+} on a 250 bp restriction fragment with irradiation at 365 nm. The pattern of oxidation was the same across the entire fragment for both agents (not shown). Both preferentially oxidize the

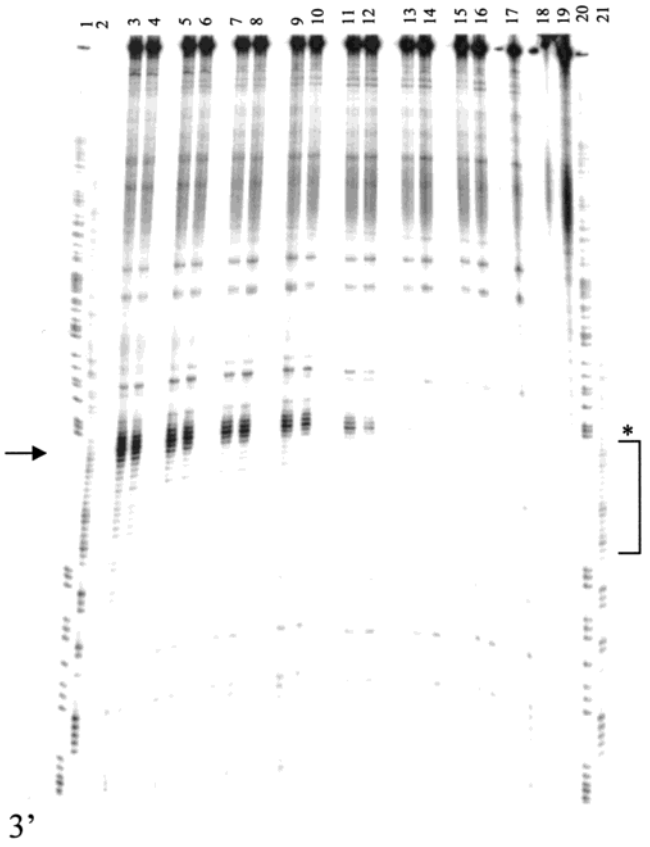

FIGURE 3: Direct photocleavage with 313 nm irradiation of a restriction fragment from the polypurine strand containing sequence 1 by Rh(phi)$_2$bpy′$^{3+}$ covalently tethered to a triplex-forming oligonucleotide. Samples contained the following concentrations of Rh-TFO, in lanes 3−17, respectively: 8 μM, 4 μM, 2 μM, 1 μM, 500 nM, 250 nM, 125 nM, 63 nM, 32 nM, 16 nM, 8 nM, 4 nM, 2 nM, 1 nM, and 0 nM. Samples were prepared in MES buffer (pH 7.0). Other conditions are as described in Materials and Methods. Maxam−Gilbert purine-specific sequencing reaction mixtures were loaded in lanes 2 and 21, and pyrimidine-specific sequencing reaction mixtures in lanes 1 and 20; lane 18 is a light control, and lane 19 is a dark control. The designed binding site is indicated by a bracket and the binding site of the appended metal by an asterisk. The arrow points to the site of direct photocleavage by the photoexcited metallointercalator.

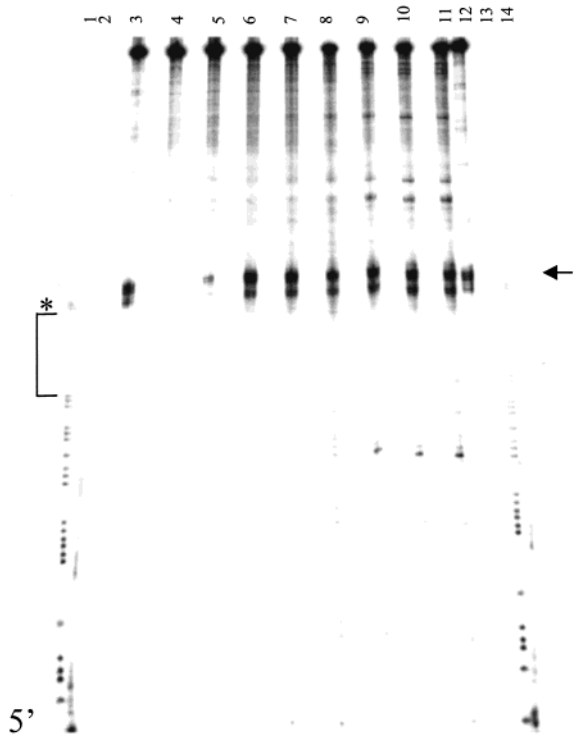

FIGURE 4: Oxidation of a restriction fragment from the pyrimidine strand of sequence 1 by $Rh(phi)_2bpy'^{3+}$ covalently tethered to a triplex-forming oligonucleotide and irradiated at 365 nm. Samples were prepared in MES buffer (pH 5.75). Other conditions are as described in Materials and Methods. Minimal long-range damage is observed at a range of irradiation times (lanes 4−11, irradiation at 365 nm for 0, 15, 30, 45, 60, 75, 90, and 120 min, respectively), although the TFO is bound to its designed site (lanes 3 and 12, irradiation at 313 nm). The site of oxidation is indicated by an arrow, while the designed TFO binding site is marked by a bracket with an asterisk indicating the binding site of the metallointercalator.

5′ guanine of 5′-GG-3′ steps, a characteristic "signature" of electron transfer.

Long-Range Oxidative Damage to Guanine by NDI in Restriction Fragments. Having demonstrated that an intercalator can be delivered to a specific site on our designed restriction fragments by covalent attachment of a triplex-forming oligonucleotide, we then explored whether NDI might be applied to examine the distance range and sequence effects for charge transfer in a restriction fragment. With the 5′-tethered NDI triplex-forming oligonucleotide, oxidative damage occurred predominantly at the intercalation site (not shown), just as we had observed with $Rh(phi)_2bpy'^{3+}$ appended to the 5′ terminus of the pyrimidine third strand. To improve the electronic coupling of the intercalator into the duplex π stack, we constructed a new NDI-tethered triplex-forming oligonucleotide with the naphthalene moiety attached to an internal cytosine residue. In this new construct, the intercalator clearly binds at a different location and possibly with a different geometry than the 5′-appended intercalators. The sequence of the 16-mer pyrimidine strand with the internal NDI was similar to that of the 5′-tethered NDI conjugate, except for the placement of the NDI intercalator and replacement of 5-methylcytosine by cytosine for synthetic reasons (Figure 2). The same target sequences were used as well, since all of the TFOs were designed to target one site.

With the internally tethered NDI, we observed strong oxidation at a distance of approximately 100 Å from the site

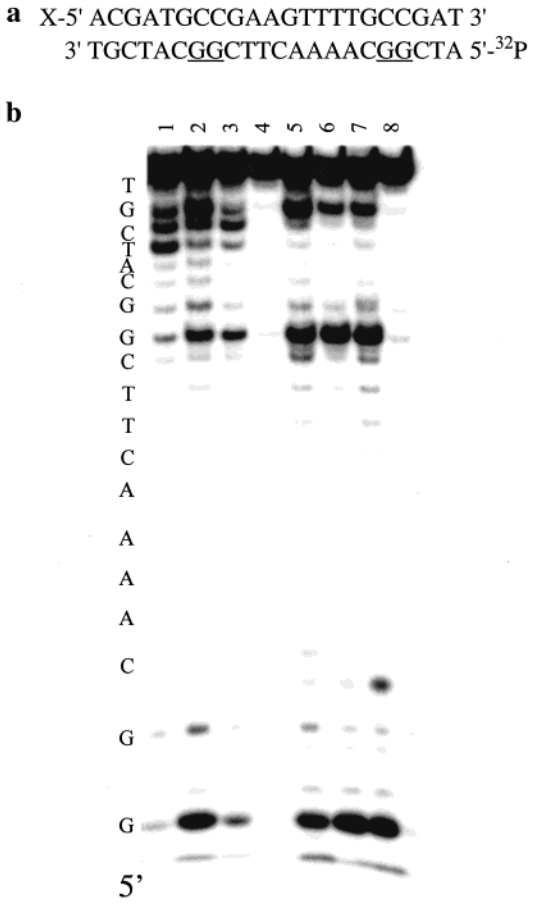

FIGURE 5: Oxidation of a short oligonucleotide duplex by noncovalent NDI. (a) Sequence of the 22 bp duplex oligonucleotide. The rhodium intercalator is tethered to the 5′ end of the top strand, indicated by an "X", where applicable. (b) Piperidine-sensitive base damage generated by covalently tethered $Rh(phi)_2bpy'^{3+}$ and noncovalent NDI: lane 1, Rh-22-mer, irradiated at 313 nm to reveal the location of intercalation; lane 2, Rh-22-mer, irradiated at 365 nm to initiate long-range oxidative base chemistry; lane 3, Rh-22-mer and noncovalent NDI, irradiated at 365 nm; lane 4, Rh-22-mer dark control; lane 5, 22-mer and noncovalent NDI, irradiated at 313 nm; lane 6, 22-mer and noncovalent NDI, irradiated at 340 nm; lane 7, 22-mer and noncovalent NDI, irradiated at 365 nm; and lane 8, 22-mer and noncovalent NDI, irradiated at 400 nm. Samples contained 2.5 μM duplex and 2.5 μM NDI, if applicable, in 35 mM Tris-HCl (pH 8.3) with 10 mM NaCl. All samples were irradiated for 1 h at room temperature.

of intercalation in both directions and along both duplex strands in the restriction fragments containing the target site (Figures 6−8). Damage occurred almost exclusively at the 5′ guanines of 5′-GG-3′ and, to a lesser extent, 5′-GA-3′ sites. Furthermore, the naphthalene-induced damage at guanine occurred with high efficiency, since most of the duplex DNA was cleaved within ∼10 min of irradiation. Minimal background damage was observed in the control sequences lacking the TFO binding site. The pattern of oxidative damage promoted by the triplex-directed naphthalene diimide intercalators on both restriction fragments is summarized in Figure 9.

More specifically, on the polypyrimidine strand of the restriction fragment containing sequence 2 (the duplex strand complementary to the polypurine TFO target strand), we observe strong guanine oxidation at the 5′ guanine of a 5′-GG-3′ site 33 bp (112 Å) away from the NDI-tethered cytosine, 3′ to the triplex region (Figures 6 and 9). Guanine

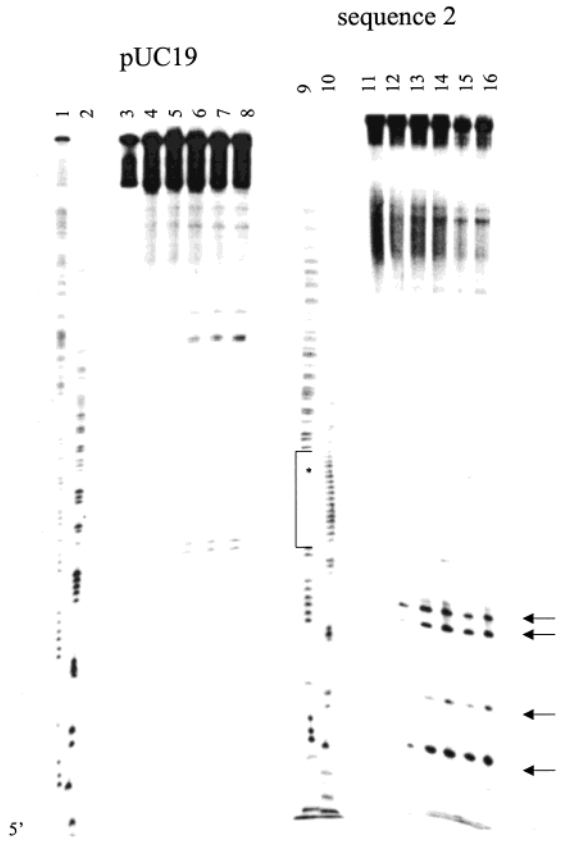

FIGURE 6: Long-range oxidation of guanine bases by the triplex-directed NDI intercalator. On the pyrimidine target strand of sequence 2 and a control fragment from pUC19. Lanes 1, 2, 9, and 10 are Maxam−Gilbert sequencing lanes. Samples in the remaining lanes were irradiated at 11 °C for different lengths of time at 365 nm, as follows: 0, 1, 2, 5, 10, and 15 min. Other conditions are as described in Materials and Methods. The region 3′ to the triplex is shown toward the top of the gel and the 5′ region toward the bottom. The location of the triplex-forming target site is indicated by a bracket, and the putative intercalation site is indicated by an asterisk. Arrows point to the sites of significant base oxidation by the NDI-tethered TFO. Minimal damage is observed in the pUC19 control fragment that does not contain a binding site.

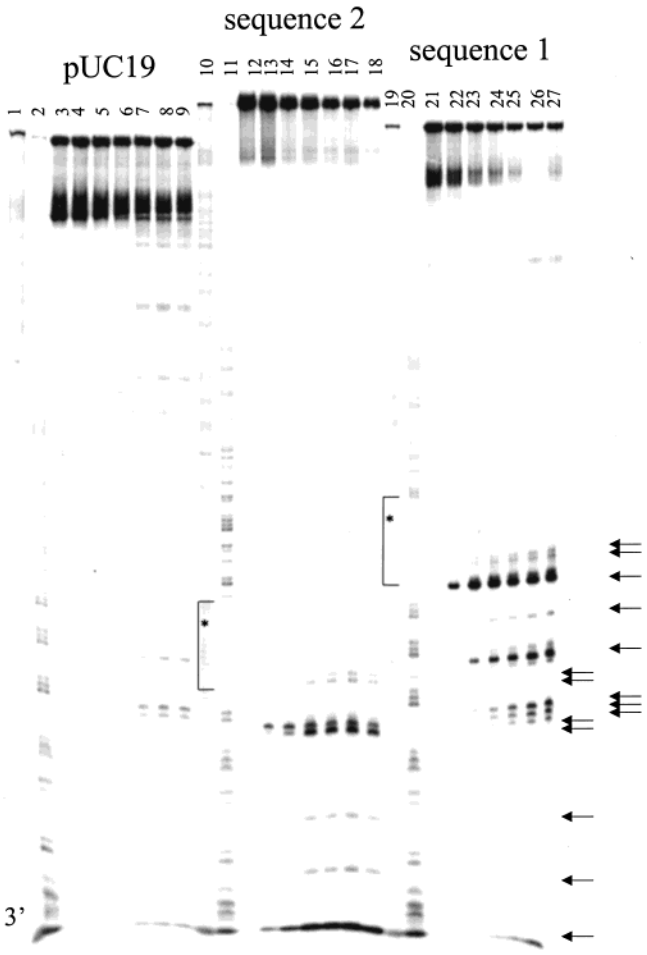

FIGURE 7: Oxidation of guanine bases on the purine strand containing sequences 1 and 2 and the pUC19 control fragment. Lanes 1, 2, 10, 11, 19, and 20 contained Maxam−Gilbert sequencing lanes. Lanes 3−9, 12−18, and 21−26 contained samples at 11 °C irradiated at 365 nm for varying lengths of time, as follows: 0, 1, 2, 4, 7, 10, and 15 min, respectively. Other conditions are as described in Materials and Methods. The region 5′ to the triplex is shown toward the top of the gel and the 3′ region toward the bottom. The location of the triplex-forming target site is indicated by a bracket, and the putative intercalation site is indicated by an asterisk. Arrows at the right point to damage in the fragment containing sequence 2; arrows at the far right point to damage in the fragment containing sequence 1. Only minimal damage is observed in the pUC19 control fragment that does not contain a binding site.

oxidation is also observed at a 5′-GGG-3′ triplet ~20 bp away and, to a lesser extent, at two intervening single guanines. Weaker oxidation beyond that point probably occurs as well, although it is difficult to quantify relative to background damage. No guanine oxidation is evident in the triplex region, since the sequence on this strand is composed entirely of pyrimidines. No oxidative base damage occurs to the 5′ side of the triplex region either; although several 5′-GG-3′ sinks are present in this region, all are located on the complementary strand. The absence of oxidative damage either within or 5′ to the triplex region was confirmed on another restriction fragment containing sequence 2 that was radiolabeled at a different restriction site (not shown).

On the target polypurine strand of sequence 2 (Figures 7 and 9), the strongest oxidation is observed at a guanine doublet 15 bp removed from the binding site on the 3′ side of the triplex, with weaker damage observed at the 5′-GG-3′ site within the triplex and at other single-guanine sites. There is also strong damage at a distal guanine doublet located ~38 bp from NDI, as judged from the intense band of small fragments at the bottom of the gel. The location and sequence of this distal cleavage site were confirmed on another restriction fragment containing sequence 2 radiolabeled at a different restriction site (Figures 8 and 9).

Because the intense cleavage 3′ to the triplex region masked any other concurrent damage further up on the gel, we isolated a slightly different restriction fragment containing sequence 2 and radioactively labeled it at the opposite side of the triplex-forming region (Figures 8 and 9). In this case, we observed significant oxidative damage on the polypurine strand within the triplex region itself. The strongest piperidine-exposed cleavage occurred at the guanine doublet immediately adjacent to the triplex region at the 3′ triplex−duplex junction (15 bp away from the intercalated NDI). Less damage was observed at the guanine doublet within the triplex region and at the guanine immediately adjacent to the intercalator itself. Minimal oxidation was observed at the guanine doublets 16 and 26 bp away that are 5′ to the triplex region.

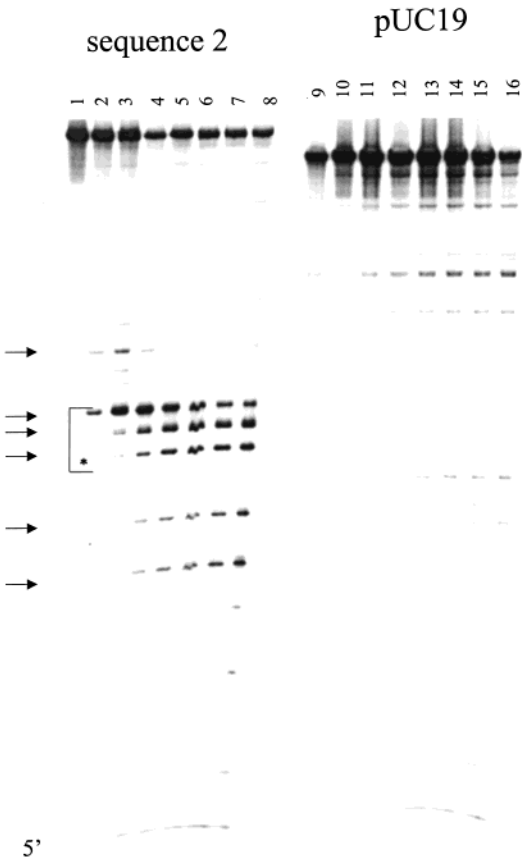

FIGURE 8: Oxidation of guanine bases on the purine strand containing sequence 2 and the pUC19 control fragment. Maxam−Gilbert sequencing lanes are not shown due to poor color contrast. Samples at 11 °C were irradiated at 365 nm for varying lengths of time, as follows: 0, 1, 2, 4, 6, 8, 10, and 12 min, respectively. Other conditions are as described in Materials and Methods. The region 5′ to the triplex is shown toward the bottom of the gel and the 3′ region toward the top. The location of the triplex-forming target site is indicated by a bracket, and the putative intercalation site is indicated by an asterisk. Arrows at the left point to damage on the fragment containing sequence 2. Background damage is observed in the pUC19 control fragment.

By comparison, on the target polypurine strand of a restriction fragment containing sequence 1, extremely intense oxidation occurs at a guanine base immediately adjacent to the 3′ end of the triplex region, 12 bases away from the NDI-tethered cytosine (Figures 7 and 9). Fairly strong damage is also seen at the 5′ guanine of a 5′-GG-3′ site 24−25 bases from the intercalator, and at a 5′-GGGG-3′ site 31−34 bases from the intercalator. The 5′-GG-3′ site inside of the triplex region also appears to be somewhat damaged. However, it is difficult to quantify any of the damage within or 5′ to the triplex region since most of the strands are cleaved in more than one place, and only the shortest piece which retains the radioactive end label appears on the gel. On the polypyrimidine strand of a restriction fragment containing sequence 1, the NDI intercalator oxidizes the guanine base immediately adjacent to the triplex on the 5′ end (data not shown). This guanine at the duplex−triplex junction is very heavily oxidized. It appears that no other bases 5′ to the triplex region are oxidized, although this absence of oxidation could not be confirmed by labeling at another restriction site, as no other restriction sites were available 5′ to the triplex region. On this polypyrimidine strand of sequence 1, the NDI intercalator also oxidizes a 5′-GGG-3′ site ~30 bp from the intercalator to the 3′ side of the triplex and two intervening single-guanine bases.

We have observed that some of the NDI-tethered oligonucleotides, in sharp contrast to metallointercalator-tethered oligonucleotides, can aggregate and can also bind nonspecifically at concentrations where all of the specific target sites are saturated. Furthermore, NDI-tethered oligonucleotides are subject to some photodecomposition when irradiated in oxygen. Therefore, it was critical in each system to test for any possibility of intermolecular reactions or nonspecific binding. In the case of our internally tethered NDI triplex-forming oligonucleotides, we observed little or no damage in the pUC restriction fragments which lack a specific binding site (Figures 7−9). This control indicates that neither free NDI, potentially generated by photodecomposition, nor stray NDI-TFO is binding nonspecifically to the restriction fragments. Moreover, it is apparent that the distribution of damage around the triplex site is markedly asymmetrical (Figure 9), further evidence that a model in which NDI is released and diffuses away cannot explain the long-range damage that we observe.

DISCUSSION

Triplex Formation, Site-Specific Delivery of Rhodium Intercalator, and Base Oxidation. It has been shown previously that polypyrimidine triplex-forming strands can be used to deliver a variety of small molecules to long DNA duplexes (*38*, *39*, *46)*. In general, the addition of an appended nonspecific intercalator improves the binding constant of the triplex-forming strand but does not change its inherent sequence specificity. In the study presented here, we observed, using DNase I footprinting and exploiting the direct strand scission chemistry of the phi complexes of rhodium, that a pyrimidine TFO can deliver a 5′-appended rhodium intercalator to a specific site within a ~250 bp restriction fragment (Figure 3). When we irradiated these samples at 365 nm to initiate long-range damage to guanine, however, we observed damage only locally (Figure 4). It was therefore apparent that the metallointercalator, delivered by triplex formation, was not well-coupled into the π stack of the restriction fragment. Interestingly, systematic changes to the intercalator and the intercalation site were insufficient to improve the electronic coupling. Since we could not determine whether the absence of long-range damage was due to poor intercalation by the octahedral complexes or to an unusual structure in the DNA duplex, we examined next whether a planar, extremely hydrophobic, organic intercalating photooxidant, covalently attached to the terminus of the sugar−phosphate backbone or to a methylated cytosine embedded in the oligonucleotide sequence, might promote long-range charge transport in restriction fragments using the triplex-directed binding methodology.

Naphthalene Diimide Intercalation. It is clear that oligonucleotide-tethered naphthalene diimide molecules can oxidize guanine at long range by charge transport through the DNA base stack. The deep intercalation of NDI within a triplex or duplex is likely advantageous in promoting long-range charge transport. Almost 20 years ago, it was shown spectroscopically and viscometrically that naphthalene diimides bind to DNA by intercalation (*23*). Later work revealed that alkylamino-substituted diimides intercalate by

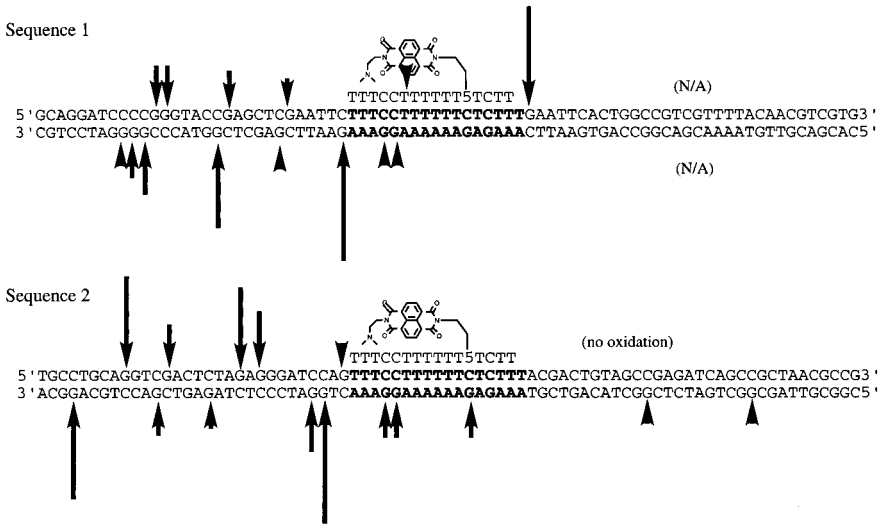

FIGURE 9: Histogram showing sites of significant base oxidation by triplex-directed naphthalene diimides on restriction fragments containing sequences 1 and 2. The sizes of the arrows reflect the relative amounts of damage generated at various guanine bases, although such measurements are merely an approximation since the data from several different gels were combined to make this histogram. Base oxidation is observed almost exclusively at guanine bases of 5′-GG-3′ or 5′-GA-3′ sites, which is characteristic of electron transfer damage through the π stack. Minimal oxidation is observed 5′ to the triplex region containing sequence 2. It is unclear whether significant oxidation is observed 5′ to the triplex region containing sequence 1 due to the large amounts of oxidized guanine generated at other guanine bases, which mask damage in this region on the gel. The triplex-forming strand is shown adjacent to the target polypyrimidine strand to make space for the arrows.

a threading mechanism in which one of the substituents must slide between the base pairs (*22*). This binding mode results in a DNA binding affinity on the order of other planar, aromatic intercalators, such as ethidium, but with association and dissociation kinetics that are considerably slower. More recently, it was shown that this favorable stacking interaction with DNA can be exploited to stabilize triplex formation (*40*). NDI hairpin linkers can be used to stabilize duplex and triplex formation by end capping, as shown by the increased melting temperatures relative to those of the same hairpins with hexa(ethylene glycol) linkers. Furthermore, NDI intercalators attached to cytosine residues within a triplex-forming strand can dramatically improve the melting temperature of a triplex (*41*). Similar NDI conjugates incorporated at the 3′ or 5′ termini (or both) of the third strand give rise to increased triplex stability, presumably as the result of intercalation into the base pairs of the target duplex (*41*, *42*). This extensive evidence of the intimate association between NDI and the DNA base pairs confirms that that they are well coupled into the DNA base stack and hence effective participants in charge transport chemistry.

Oxidation by Naphthalene Diimide Intercalators. Photoexcited naphthalene diimides are powerful oxidants, estimated to have a reduction potential around 1.8 V versus NHE (*31*, *32*). They have been used recently in several model studies of electron transfer between tethered donor and acceptor molecules (*24*−*28*). On the basis of a careful photophysical characterization of NDI in solution and the somewhat contradictory evidence for guanine oxidation by related molecules available in the literature, Aveline et al. proposed the following mechanism for the interaction of NDI with DNA (*47*); upon photoexcitation at 355 nm, the excited singlet species can produce hydroxyl radicals or undergo a rapid intersystem crossing to the excited triplet species. The excited-state triplet can then oxidize another NDI molecule or some other available electron donor or generate singlet oxygen. In our system, the hydroperoxy group which forms hydroxyl radicals is absent, and on average, only one NDI molecule is present per duplex, eliminating two of these possible reaction pathways. The best available electron donor in the native DNA duplex is guanine. We propose that irradiation of NDI in our system leads to oxidation of guanine or the generation of singlet oxygen. In oligonucleotide duplexes and restriction fragments irradiated with noncovalent NDI, we observe oxidation of guanine with a strong preference for 5′ guanines of 5′-GG-3′ doublets (Figure 5). This damage pattern is consistent with electron transfer processes but is inconsistent with damage from singlet oxygen (*2*, *6*).

Probing Triplex Structure Using Long-Range Charge Transfer. The NDI intercalator, delivered specifically to a single site, was used to probe the structure of triplex regions and examine long-range charge transport in restriction fragments. We have shown that long-range charge transfer initiated by photoexcited $Rh(phi)_2bpy'^{3+}$ could be used to probe the structure of DNA−protein complexes; the extent of charge transfer through the base stack was diminished upon binding of a protein which disturbed π stacking in a base-flipping reaction (*48*). Here charge transport through the base stack initiated by photoexcited NDI yields insights into the structure of the triplex region and its effect upon neighboring duplex regions. We observe that in general charge moves through the triplex region to the duplex, resulting in significant oxidation at a distance from the intercalation site, which lies within the triplex (Figure 9). Consequently, it is clear that the bases within the triplex region are well-stacked with each other and with the duplex region to the 3′ side. This conclusion is consistent with NMR solution structures of intramolecular triplex hairpins showing such base stacking (albeit neither B- nor A-form) (*49*−*51*).

In contrast to the large amounts of oxidative damage on the 3′ side of the triplex site, oxidation to the 5′ side of the triplex is minimal. This becomes important to consider in the context of observations that very little long-range

oxidation is observed with 5′-appended oxidants, both NDI (not shown) and $Rh(phi)_2bpy'^{3+}$ (Figure 4). Similar results have been reported previously with a 5′-appended flavin TFO (*52*). Thus, it appears that the triplex region is not well-stacked with the duplex region to the 5′ side, i.e., that there is a junction between the two regions where the bases do not overlap. The junction effect is directional, in that the duplex−triplex stacking on the 3′ side appears to be effective and on the 5′ side appears to be poor. This hypothesis explains why several 5′-tethered intercalators do not oxidize guanine bases at long range, but an internally tethered NDI can do so.

The observation that the duplex−triplex region is poorly stacked is actually also consistent with previous results which showed poor charge transfer through 5′-TA-3′ steps (*8*). Generally, one expects that 5′-pyrimidine-purine-3′ steps provide less efficient charge transport because of the diminished π overlap between the pyrimidine and purine base pairs, theoretically inhibiting coupling and surely increasing the probability of kinked structures and dynamic bending (*53*). In contrast, 5′-purine-pyrimidine-3′ steps display significantly more overlap due to the helical twist of the DNA. A 5′-pyrimidine-purine-3′ step is present at the 5′ duplex−triplex junction in both plasmid 1 and 2, whereas a 5′-purine-pyrimidine-3′ step exists at the 3′ junction, leading us to expect a more continuous transition between triplex and duplex at the 3′ junction than at the 5′ end. Obviously, it is important not to overemphasize this effect, since both sequences abound with 5′-pyrimidine-purine-3′ steps which do not appear to reduce the extent of charge transfer significantly. Any discontinuity in the base−base stacking at the duplex−triplex junction is generated by the unusual stacking in the triplex region which does not overlap well with the bases of the duplex region, and the discontinuity may be merely exacerbated or localized by the inherently poor stacking of a 5′-pyrimidine-purine-3′ step. The information concerning stacking at duplex−triplex junctions gleaned from this charge transport study is especially valuable in light of the fact that little or no structural information about such junctions is available currently (*54*). Indeed, measurements of charge transport provide a novel and sensitive probe of DNA stacking and dynamics.

Clearly, less oxidative damage arises within the triplex region compared to the distal duplex region. It has been proposed that this reduced yield of oxidized guanine within a triplex could be due to (i) the effect of reduced oxygen accessibility and trapping, (ii) the effect of altered stacking on the redox potentials and charge stabilization of guanine doublets, or (iii) the effect of protonated cytosine bases on the electronic structure of the guanine bases (*55*). The first suggestion is almost certainly true, given that the major groove is occupied by the triplex-forming strand and ordered water molecules, which must reduce oxygen accessibility. Since the stacking of the bases is not substantially altered compared to that in canonical B-form DNA (*49*−*51*), and since the differences in potential generated by stacking interactions are likely to be small (*4*), it is unlikely that the oxidation potential could be perturbed sufficiently to grossly disturb guanine oxidation in the triplex region; it may account for a small fraction of the diminution. The third proposal is also plausible, but the effect of a protonated third strand on the electronic structure of the duplex should be experimentally accessible via comparison of charge transfer through purine versus pyrimidine triplexes.

In and around the triplex region, guanine bases on both strands of the duplex are damaged. This observation is especially interesting when we consider that in the triplex region, between 17 and 20 continuous purine bases are found on one strand and the complementary continuous string of pyrimidines is found on the other. The fact that guanine bases on both strands are damaged implies that migrating charges can move from one strand of the duplex to the other, and we have previously observed interstrand charge transfer in spectroscopic studies (*56*). Alternatively, our results may imply that charges can move through long stretches of pyrimidine bases as well as through purine bases, since significant damage is observed on the pyrimidine duplex strand.

These results and their implications for the structure of a DNA triplex appear to be fairly consistent with recent work of Kan et al. on guanine oxidation by anthraquinones on short oligonucleotide triplexes (*55*). However, our system in which the NDI chromophore is delivered to a restriction fragment by a TFO offers important new insights. Since oxidation in the NDI-tethered triplex system was monitored on both the polypurine and polypyrimidine strands of the duplex, we can assess charge transport through polypyrimidine sequences. Furthermore, since our experiments exploited restriction fragments instead of short oligonucleotide duplexes, the ability of the NDI-tethered TFO to find its target site within a long genomic sequence was established. Most importantly, the targeting of guanine damage in restriction fragments with random DNA sequences by triplex formation provides a strategy for probing long-range charge transfer and base oxidation in genomic DNA, a critical issue in assessing the physiological consequences of DNA-mediated electron transfer.

Long-Range Oxidation in Restriction Fragments. Using specific triplex formation as a means of delivering a photooxidant to a specific location on a long DNA duplex, we have now observed charge transfer to damage guanines at long range, over roughly 25−38 bp in each direction, or approximately 70 bp total. The triplex delivery system allows us to examine for the first time charge transfer to damage guanine on both strands of the DNA duplex, confirming that oxidized guanine is generated on both strands with a similar distance range for its distribution. This distribution of oxidized bases seen here provides an example of the distance range for charge transport in a random sequence restriction fragment. This range appears to be about half of what we had previously observed on a synthetic oligonucleotide construct (*8*). However, here the charge can migrate in two directions, which should on average cut in half the signal at the distal sites, and the weaker damage is more difficult to measure due to background from nonspecific binding and the possible distribution of very long-range damage among many distal sites. Base damage is therefore seen to be distributed over about 70 bp (∼235 Å). This overall distance distribution for charge transport is roughly comparable to what we have observed previously in one direction on oligonucleotides. It is interesting to consider whether this distance, roughly equal to one loop around a nucleosome, may therefore represent the distance regime to consider for chemical communication using DNA-mediated charge transport (*20*).

CONCLUSIONS

Naphthalene diimide intercalators are efficient long-range DNA photooxidants. When covalently tethered to a triplex-forming oligonucleotide, they can be delivered to a single specific site on a restriction fragment. Triplex-directed NDI intercalators were used to demonstrate that charges can migrate through genomic DNA over 25−34 bp in both directions down the helix and along both duplex strands, to generate permanent base lesions. The potential now exists to examine long-range charge transport in a variety of biological systems, including supercoiled plasmids, mammalian chromosomal DNA, and even inside of cells, to examine the biological relevance and implications of DNA-mediated charge transport in vivo.

ACKNOWLEDGMENT

We thank William Greenberg for his helpful suggestions.

REFERENCES

1. Kelley, S. O., and Barton, J. K. (1998) in *Metal Ions in Biological Systems* (Sigel, A., and Sigel, H., Eds.) pp 211−249, Marcel Dekker, New York.
2. Hall, D. B., Holmlin, R. E., and Barton, J. K. (1996) *Nature 382*, 731−735.
3. Steenken, S., and Jovanovic, S. V. (1997) *J. Am. Chem. Soc. 119*, 617−618.
4. Sugiyama, H., and Saito, I. (1996) *J. Am. Chem. Soc. 118*, 7063−7064.
5. Prat, F., Houk, K. N., and Foote, C. S. (1998) *J. Am. Chem. Soc. 120*, 845−846.
6. Burrows, C. J., and Muller, J. G. (1998) *Chem. Rev. 98*, 1109−1151.
7. Hall, D. B., and Barton, J. K. (1997) *J. Am. Chem. Soc. 119*, 5045−5046.
8. Núñez, M., Hall, D., and Barton, J. K. (1999) *Chem. Biol. 6*, 85−97.
9. Arkin, M. R., Stemp, E. D. A., Coates Pulver, S., and Barton, J. K. (1997) *Chem. Biol. 4*, 389−400.
10. Hall, D. B., Kelley, S. O., and Barton, J. K. (1998) *Biochemistry 37*, 15933−15940.
11. Henderson, P. T., Jones, D., Hampikian, G., Kan, Y., and Schuster, G. (1999) *Proc. Natl. Acad. Sci. U.S.A. 96*, 8353−8358.
12. Gasper, S. M., and Schuster, G. B. (1997) *J. Am. Chem. Soc. 119*, 12762−12771.
13. Bixon, M., Giese, B., Wessely, B., Langenbacher, T., Michel-Beyerle, M. E., and Jortner, J. (1999) *Proc. Natl. Acad. Sci. U.S.A. 96*, 11713−11716.
14. Núñez, M. E., and Barton, J. K. (2000) *Curr. Opin. Chem. Biol. 4*, 199−206.
15. Stemp, E. D. A., Arkin, M. R., and Barton, J. K. (1997) *J. Am. Chem. Soc. 119*, 2921−2925.
16. Burrows, C. J., and Muller, J. G. (1998) *Chem. Rev. 98*, 1109−1151.
17. Buchko, G. W., Wagner, J. R., Cadet, J., Raoul, S., and Weinfeld, M. (1995) *Biochim. Biophys. Acta 1263*, 17−24.
18. Muller, J. G., Duarte, V., Hickerson, R. P., and Burrows, C. J. (1998) *Nucleic Acids Res. 26*, 2247−2249.
19. Cullis, P. M., Malone, M. E., and Merson-Davies, L. A. (1996) *J. Am. Chem. Soc. 118*, 2775−2781.
20. Rajski, S. R., Jackson, B. A., and Barton, J. K. (2000) *Mutat. Res. 447*, 49−72.
21. Liu, Z.-R., Hecker, K. H., and Rill, R. L. (1996) *J. Biomol. Struct. Dyn. 14*, 331−339.
22. Tanious, F. A., Yen, S.-F., and Wilson, W. D. (1991) *Biochemistry 30*, 1813−1819.
23. Yen, S.-F., Gabbay, E. J., and Wilson, W. D. (1982) *Biochemistry 21*, 2070−2076.
24. Lokey, R. S., Kwok, Y., Guelev, V., Pursell, C. J., Hurley, L. H., and Iverson, B. L. (1997) *J. Am. Chem. Soc. 119*, 7202−7210.
25. Sessler, J. L., Brown, C. T., O'Connor, D., Springs, S. L., Wang, R., Sathiosatham, M., and Hirose, T. (1998) *J. Org. Chem. 63*, 7370−7374.
26. Tan, Q., Kuciauskas, D., Lin, S., Stone, S., Moore, A. L., Moore, T. A., and Gust, D. (1997) *J. Phys. Chem. B 101*, 5214−5223.
27. Levanon, H., Galili, T., Regev, A., Wiederrecht, G. P., Svec, W. A., and Wasielewski, M. R. (1998) *J. Am. Chem. Soc. 120*, 6366−6373.
28. Miller, L. L., and Mann, K. R. (1996) *Acc. Chem. Res. 29*, 417−423.
29. Matsugo, S., Kawanishi, S., Yamamoto, K., Sugiyama, H., Matsuura, T., and Saito, I. (1991) *Angew. Chem., Int. Ed. Engl. 30*, 1351−1353.
30. Saito, I., Takayama, M., Sugiyama, H., Nakatani, K., Tsuchida, A., and Yamamoto, M. (1995) *J. Am. Chem. Soc. 117*, 6406−6407.
31. Rogers, J. E., and Kelly, L. A. (1999) *J. Am. Chem. Soc. 121*, 3854−3861.
32. Rogers, J. E., Weiss, S. J., and Kelly, L. A. (2000) *J. Am. Chem. Soc. 122*, 427−436.
33. Saenger, W. (1984) *Principles of Nucleic Acid Structure*, Springer-Verlag, New York.
34. Moser, H. E., and Dervan, P. B. (1987) *Science 238*, 645−650.
35. Strobel, S., and Dervan, P. B. (1990) *Science 249*, 73−75.
36. Greenberg, W., and Dervan, P. B. (1995) *J. Am. Chem. Soc. 117*, 5016−5022.
37. Best, G. C., and Dervan, P. B. (1995) *J. Am. Chem. Soc. 117*, 1187−1193.
38. Dervan, P. B. (1992) *Nature 359*, 87−88.
39. Sun, J.-S., Garestier, T., and Hélène, C. (1996) *Curr. Opin. Struct. Biol. 6*, 327−333.
40. Bevers, S., O'Dea, T., and McLaughlin, L. (1998) *J. Am. Chem. Soc. 120*, 11004−11005.
41. Gianolio, D., and McLaughlin, L. (1999) *J. Am. Chem. Soc. 121*, 6334−6335.
42. Gianolio, D., Segismundo, J., and McLaughlin, L. W. (2000) *Nucleic Acids Res. 28*, 2128−2134.
43. Núñez, M., Rajski, S. R., and Barton, J. K. (2000) *Methods Enzymol.* (in press).
44. Sambrook, J., Fritsch, E. F., and Maniatis, T. (1989) *Molecular Cloning: A Laboratory Manual*, 2nd ed., Cold Spring Harbor Laboratory Press, Plainview, NY.
45. Sitlani, A., and Barton, J. K. (1994) *Biochemistry 33*, 12100−12108.
46. Grigoriev, M., Praseuth, D., Robin, P., Hemar, A., Saison-Behmoaras, T., Dautry-Varsat, A., Thuong, N. T., Hélène, C., and Harel-Bellan, A. (1992) *J. Biol. Chem. 267*, 3389−3395.
47. Aveline, B. M., Matusgo, S., and Redmond, R. W. (1997) *J. Am. Chem. Soc. 119*, 11785−11795.
48. Rajski, S. R., Kumar, S., Roberts, R. J., and Barton, J. K. (1999) *J. Am. Chem. Soc. 121*, 5615−5616.
49. Radhakrishnan, I., and Patel, D. J. (1994) *Biochemistry 33*, 11405−11416.
50. Tarköy, M., Phipps, A. K., Shultze, P., and Feigon, J. (1998) *Biochemistry 37*, 5810−5819.
51. Radhikrishnan, I., and Patel, D. J. (1994) *Structure 2*, 17−32.
52. Frier, C., Mouscadet, J.-F., Décout, J.-L., Auclair, C., and Fontecave, M. (1998) *Chem. Commun. 22*, 2457−2458.
53. Dickerson, R. E. (1998) *Nucleic Acids Res. 26*, 1906−1926.
54. Rhee, S., Han, Z., Liu, K., Miles, T., and Davies, D. R. (1999) *Biochemistry 38*, 16810−16815.
55. Kan, Y., and Schuster, G. B. (1999) *J. Am. Chem. Soc. 121*, 10857−10864.
56. Kelley, S. O., and Barton, J. K. (1999) *Science 283*, 375−381.

BI000285S